JOURNAL OF PROPULSION AND POWER
Vol. 10, No. 5, Sept.–Oct. 1994

Single-Passage Euler Analysis of Oscillating Cascade Aerodynamics for Arbitrary Interblade Phase

James M. Wolff* and Sanford Fleeter†
Purdue University, West Lafayette, Indiana 47907

The unsteady flowfield through a harmonically oscillating cascade of airfoils is investigated using a time-marching Euler code implemented on a deforming C-grid. Various methods of calculating the boundary conditions are considered, with special attention paid to the unsteady periodic boundary conditions and reducing computer resource requirements. The Euler code is then used to predict the unsteady aerodynamics for both translational and torsional cascade oscillations for several cascade flow geometries. A flat plate cascade is used to verify the flow solver with linear theory predictions. A typical compressor rotor configuration is used to introduce nonlinear effects. The effect of a strong normal shock with varied amplitudes of oscillation demonstrates the nonlinear behavior of the periodic boundary conditions and helps to define the limiting conditions for linearized analyses.

Nomenclature

C = airfoil chord
C_M = unsteady moment coefficient, $m/(C^2\rho_1 V_1^2)$
C_p = pressure coefficient, $-(p - p_1)/(\frac{1}{2}\rho_1 V_1^2)$
F, G = flux vectors
h_1 = amplitude of translational motion based on chord
k = reduced frequency, $\omega C/2V_1$
M = freestream Mach number
m = moment
N_p = number of time steps in one period of oscillation
P_0 = total pressure
p = static pressure
Q = dependent variable vector
S = cascade spacing
t, τ = time
u, v = velocities in the x and y directions
V = total velocity
x, y = spatial coordinates
α = incidence angle, deg
α_1 = amplitude of oscillation for torsional motion, deg
ΔC_p = pressure difference coefficient, $(p_L - p_U)/(\frac{1}{2}\rho_1 V_1^2 |\alpha_1|)$
ζ = cascade stagger angle, deg
ξ, η = curvilinear coordinate directions
ρ = fluid density
σ = interblade phase angle, deg
ω = angular frequency

Subscripts
L, U = upper/lower periodic boundary condition
0 = steady solution
1, 2 = inlet/exit conditions

Superscripts
n = time level index
0 = time average value

Presented as Paper 93-0389 at the AIAA 31st Aerospace Sciences Meeting and Exhibit, Reno, NV, Jan. 11–14, 1993; received April 19, 1993; revision received Dec. 13, 1993; accepted for publication Feb. 15, 1994.

*AFRAPT Trainee, School of Mechanical Engineering.
†Professor, School of Mechanical Engineering.

Introduction

UNSTEADY aerodynamic phenomena continue to produce serious aeroelastic problems in the development of new turbomachinery. To minimize this development problem, accurate unsteady aerodynamic cascade models are required. Such models are generally time linearized, with the validity of these linearized models for subsonic flows well-established for low aerodynamic loading.[1,2] However, these linearized flow models may not be valid for many situations. For example, nonlinear effects are quite likely to be associated with larger amplitudes of blade oscillation as well as unsteady transonic flows with shock motion induced by oscillating blades at small amplitudes.

To analyze nonlinear flowfields, unsteady Euler codes are being developed. Finite difference schemes[3–6] are being used to solve the Euler equations for oscillating cascades by time-marching methods. However, they require much more computer time and storage than do linearized codes. For cascade studies, an important aspect of this additional computational expense is associated with the passage periodic boundary conditions that arise from a constant interblade phase angle between adjacent oscillating airfoils. Several methods have been proposed to specify the periodic boundary condition, *a-b* and *c-d* in Fig. 1.

The simplest method is to "stack" airfoil grids and pass information between adjacent grids. This is accomplished by expanding the grids so that they overlap along the periodic boundaries (Fig. 1). The solution is marched globally in time with each passage's blade moving with a different phase angle. The solution at the periodic boundaries is then determined as part of the interior solution. With the airfoils oscillating at a fixed nonzero interblade phase angle, the minimum number of airfoils N_α that satisfies the periodicity requirement is

$$N_\alpha |\sigma| = 360 \text{ deg} \tag{1}$$

A 90-deg interblade phase angle analysis thus requires modeling four airfoils and four flow passages. Although numerically accurate, this method requires additional computational time for nonzero interblade phase angle calculations, with some interblade phase angles practically impossible to analyze.

Single-blade passage techniques, with the periodic boundary conditions phase shifted for nonzero interblade phase angle values, minimize the computational requirements by eliminating this flow passage stacking. The direct store method, first proposed by Erdos and Alzner,[7] requires that all the

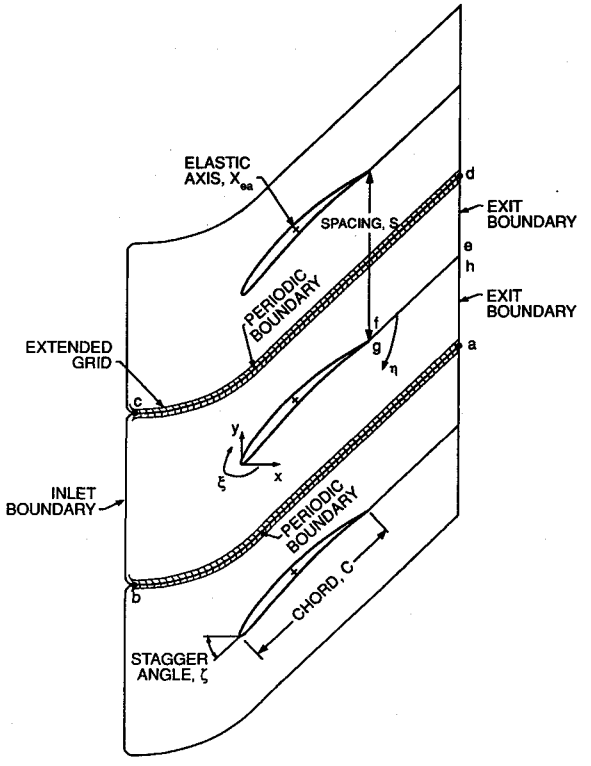

Fig. 1 Computational and cascade geometry.

dependent variables on the periodic boundaries be stored for a period of airfoil oscillation. At every time step, parameters at the boundaries are updated by averaging the data obtained from the current time-marching solution and those stored according to the given interblade phase angle. At the same time the stored parameters are updated. The periodic boundary condition is satisfied when the time marching process converges to a periodic solution. The primary disadvantage of this method is the large computer storage required, especially at low cascade oscillation frequency values.

Another single-passage approach to the problem of lagged periodic boundary conditions was developed by Giles.[8] The computational time plane was inclined in the blade pitch direction so that the solutions at the upper and lower periodic boundaries could be directly equated. The simplicity in the periodic boundary condition is achieved at the expense of modifying the basic partial differential equations in the interior of the computational domain. However, because of the characteristics of the Euler equations, the inclination angle of the computational plane was restricted to a range of phase angles. For conditions outside this range, Giles had to use multipassage conditions, which again consumed more computer time and storage.

To avoid the large computer time or memory requirements of the above noted methods, He[9] assumed a Fourier series expansion at the periodic boundaries and then lagged the boundary conditions by the interblade phase angle. In this method, the Fourier coefficients of the response at the periodic boundaries are stored and continually updated. This is more efficient in computer memory usage than that of the direct store method, which stores the entire time history at the periodic boundary. Thus, this method shows tremendous promise for conserving computer resources.

In this article, the unsteady periodic boundary conditions for unsteady Euler models are investigated, including a variation of the Fourier series lagged boundary condition originally proposed by He. The boundary conditions are implemented on an expanded grid along the periodic boundary, therefore, the periodic boundary is part of the interior solution. The two-dimensional unsteady Euler equations are solved using a time-marching, flux-difference splitting scheme implemented on a C-grid that is allowed to deform with the airfoil motion, either torsional or translational. Predictions for both flat plate and loaded airfoil cascades are then presented, with the oscillation amplitude, cascade geometry, and interblade phase angles varied.

Mathematical Model

The inviscid flowfield computations are performed using an implicit finite volume Euler scheme.[10,11] The discretized integral form of the time-dependent curvilinear Euler equations is obtained by integrating the partial differential equations over a computational volume with the center denoted as (i, j), and changing the resulting volume integral to a surface integral using the divergence theorem

$$\frac{\partial \boldsymbol{Q}}{\partial \tau} + \frac{\delta_i \boldsymbol{F}}{\Delta \xi} + \frac{\delta_j \boldsymbol{G}}{\Delta \eta} = 0 \tag{2}$$

where the central difference operators $\delta_m(\bullet) = (\bullet)_{m+1/2} - (\bullet)_{m-1/2}$, $m = i, j$ imply that the flux vectors are evaluated at the surfaces of a cell. The dissipation aspect of this scheme is improved by a flux-difference split method for the residual based on the solution of approximate Riemann problems with Roe averaging at the cell faces. To obtain higher-order spatial accuracy, a corrective flux is added with a total variational diminishing scheme used to limit the interface flux. Excellent results[10,11] have been obtained by evaluating the residual term with the flux-difference split method and the left-hand side operator with the flux vector split scheme, which is approximately factored into the product of two operators. The geometric conservation law, which prevents spurious source terms due to the motion of the grid, is satisfied resulting in a flow solver that is third-order accurate spatially and second-order accurate in time.[10,11]

The Euler numerical solution is implemented on an airfoil cascade geometry (Fig. 1) by a computational C-grid. In particular, the numerical solution is obtained utilizing the deforming grid technique of Refs. 5 and 12 for zero and nonzero interblade phase angles. The outer boundary of the C-grid is defined by the user in the grid generation program GRAPE.[13,14] The outer boundary remains fixed in space, with the deforming grid technique used to locate the position of the airfoil.

Boundary Conditions

Solid Surface

The solid surface boundary conditions, *f-g* in Fig. 1, implement zero pressure gradient conditions.[15] These zero pressure gradient boundary conditions are sufficient as long as the grid near the surface is adequately resolved. The flow variables are averaged across the interface aft of the airfoil solid surface to the exit, *e-f* and *g-h* in Fig. 1.

Inlet and Exit

Characteristic variable boundary conditions (CVBC) are used for proper transmission of information into and out, *b-c* and *d-e*, *h-a*, respectively in Fig. 1, of the steady computational domain. The CVBCs are consistent with the concept of upwinding in which the signs of the characteristic velocities determine the appropriate propagation directions.[15] Note that CVBCs are only valid for steady cascade flows because the exit boundary is assumed to have uniform static pressure.

Approximate nonreflecting unsteady inlet and exit boundary conditions are developed by assuming that linear theory can be applied. Giles[16] derived nonreflecting boundary conditions for a general turbomachinery Euler solver. First, the steady flow is solved using the CVBCs. The linearized Euler equations are then solved at the inlet and exit boundary assuming locally one-dimensional flow to determine the perturbation flow variables in terms of the characteristic varia-

bles. This allows time variations of static pressure at the exit and reduces reflections from the boundaries.

Fourier Periodic

To minimize the large computer time or memory requirements associated with implementing the periodic boundary conditions for nonzero interblade phase angle values, the flow variables at the periodic boundaries are approximately expressed as a Fourier series.[9] This is accomplished by expanding the computational grid one node at the upper and lower periodic boundaries (Fig. 1). At one node interior of the upper and lower periodic boundaries, timewise integration using rectangular rule quadrature for the Fourier coefficients are performed on the conservative variables $f(x, t)$ [$\rho(x, t)$, $\rho u(x, t)$, etc.] at the lower and upper boundaries:

Lower boundary

$$A_L^n(x) = \frac{\omega}{\pi} \sum_{n=1}^{N_p} f_{U-1}(x, t)\sin(n\omega t)\Delta t \tag{3a}$$

$$B_L^n(x) = \frac{\omega}{\pi} \sum_{n=1}^{N_p} f_{U-1}(x, t)\cos(n\omega t)\Delta t \tag{3b}$$

Upper boundary

$$A_U^n(x) = \frac{\omega}{\pi} \sum_{n=1}^{N_p} f_{L-1}(x, t)\sin(n\omega t)\Delta t \tag{3c}$$

$$B_U^n(x) = \frac{\omega}{\pi} \sum_{n=1}^{N_p} f_{L-1}(x, t)\cos(n\omega t)\Delta t \tag{3d}$$

The solutions at the overlapped nodes for the lower and upper periodic boundaries are then found by an N term timewise Fourier series for the conservative variables $f(x, t)$

$$f_{L+1}(x, t) = f_{U-1}^0(x) + \sum_{n=1}^{N} \{A_L^n(x)\sin[n(\omega t - \sigma)] + B_L^n(x)\cos[n(\omega t - \sigma)]\} \tag{4a}$$

$$f_{U+1}(x, t) = f_{L-1}^0(x) + \sum_{n=1}^{N} \{A_U^n(x)\sin[n(\omega t + \sigma)] + B_U^n(x)\cos[n(\omega t + \sigma)]\} \tag{4b}$$

where f^0 is the time-averaged value of f.

The implementation procedure for Eqs. (3) and (4) is to first perform the timewise integration for the Fourier coefficients at one node interior to the periodic boundaries. This is an interior solution from the flow solver. The current solution at the expanded nodes is then calculated using the Fourier coefficients from the previous time period and Eq. (4). After each period of integration, new values of the coefficients are obtained from Eq. (3). Then the coefficients in Eq. (4) are updated by the new values obtained. To accelerate convergence to a periodic solution, the coefficients and time-averaged values are updated five times per period of oscillation.

In this method, the Fourier coefficients of the response at the periodic boundaries are stored and continually updated. This is more efficient in computer memory usage than that of the direct store method that stores the entire time history at the periodic boundary.

To obtain coefficients for the first period of oscillation, a zero interblade phase angle configuration is analyzed with the coefficients calculated on the upper and lower boundaries and stored. For a nonzero interblade phase angle, the zero phase angle coefficients are used only for the first period with the appropriate nonzero interblade phase angle then applied. The analysis is then run until a periodic solution is achieved, which is defined by a constant unsteady moment and lift coefficient for successive periods.

Results

In this article, the unsteady periodic boundary conditions for unsteady Euler models are investigated. The two-dimensional unsteady Euler equations are solved for a cascade geometry (Fig. 1) using a time-marching, flux-difference splitting scheme implemented on a C-grid that is allowed to deform with the airfoil motion, either torsional or translational. Predictions for both flat plate and loaded oscillating airfoil cascades are presented, with the oscillation amplitude, cascade geometry, and interblade phase angles varied.

Flat Plate Results

To validate the Euler solutions, the unsteady flow past an oscillating flat plate cascade is analyzed and compared with linear theory predictions. The cascade consists of flat plates staggered at 45 deg with a solidity of 1.0. The inlet Mach number is 0.7 and the mean flow incidence angle is zero. A finite 1% thick, rounded nose airfoil is used to approximate the flat plate airfoils. A 145 × 28 C-grid is extended 0.95 chords upstream of the leading edge and 1.0 chords downstream of the trailing edge (Fig. 2a). Initially, the flow variables are set equal to the previously determined steady-state values. Then the airfoils oscillate for a number of cycles sufficient to achieve a periodic unsteady solution. The airfoil surface unsteady pressures for the last cycle of oscillation are then Fourier decomposed to determine the first harmonic unsteady pressure distribution.

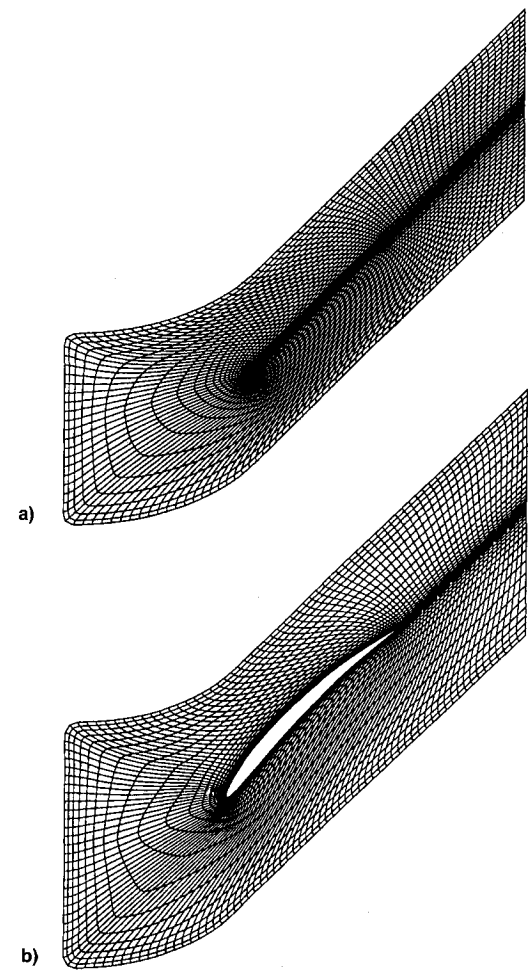

Fig. 2 Computational grids: a) flat plate and b) 10th standard configuration.

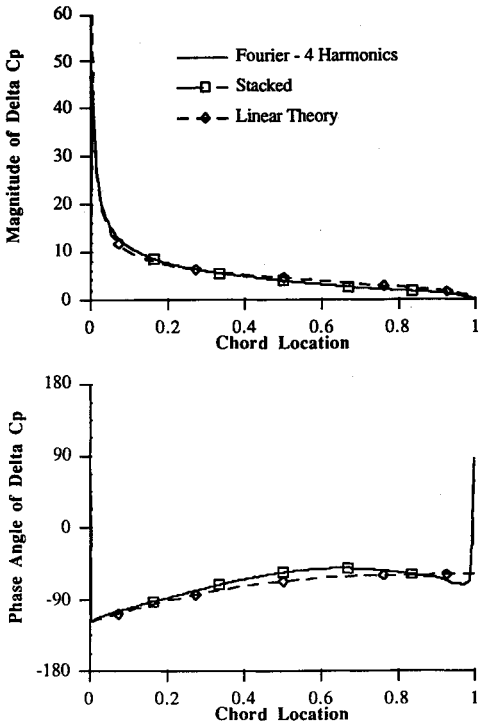

Fig. 3 Flat plate cascade unsteady pressure difference. M = 0.7, k = 0.75, ζ = 45 deg, α = 0 deg, p/P_0 = 0.721, h_1 = 0.01, C/S = 1.0, σ = 90 deg.

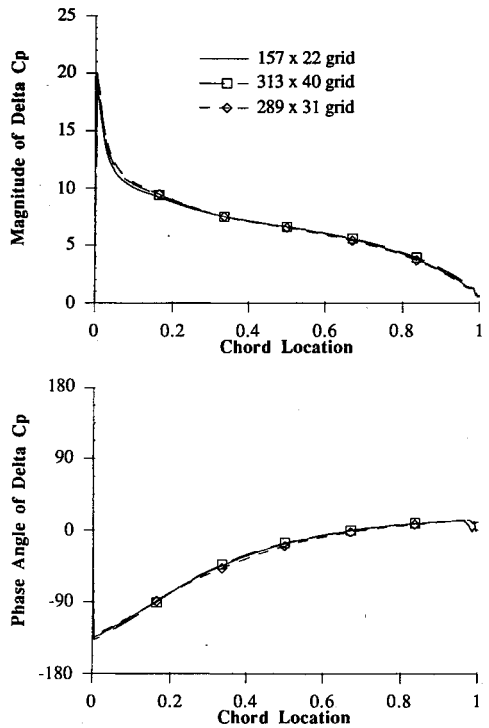

Fig. 4 Grid effect on 10th standard configuration unsteady pressure difference. M = 0.7, k = 0.75, ζ = 45 deg, α = 10 deg, p/P_0 = 0.87, h_1 = 0.01, C/S = 1.0, σ = 0 deg.

Figure 3 shows the magnitude and phase of the airfoil surface unsteady pressure response to a 1% chord translational motion at an interblade phase angle of 90 deg and a k of 0.75. The predictions of the Euler solver using the stacked and Fourier periodic boundary conditions (four harmonics) are shown. There is no difference in the response for either of the two Euler periodic boundary conditions. Excellent agreement of the unsteady pressure magnitude between the Euler predictions and the linear theory analysis of Whitehead[1] is evident. The phase distributions are also in good agreement with the linear theory predictions. From 20 to 80% chord, the Euler solver predicts a slightly higher phase angle. The large jump in phase at the trailing edge is a result of the unsteady pressure difference magnitude approaching zero, thereby making any slight difference in the unsteady pressure appear large.

The computational time for the Fourier periodic boundary condition analysis, which required seven cycles of oscillation to converge, was 5 CPU h vs 11 CPU h on a HP-730 workstation for the stacked periodic boundary condition, which converged in four oscillations.

10th Standard Configuration

To demonstrate the Fourier periodic boundary conditions for subsonic flow, a loaded airfoil cascade was analyzed. The 10th standard configuration[17] is a cascade of modified cambered NACA 0006 airfoils at 45-deg stagger, 10-deg angle of attack, with a solidity of 1.0. The unsteady cascade flow generated by translational motion is analyzed.

A grid convergence study was conducted to verify grid independent results. Figure 4 shows the unsteady magnitude and phase pressure response of the 10th standard configuration cascade oscillating with a 0.75 reduced frequency value, a freestream Mach number of 0.7, and a 0-deg interblade phase angle executing translational motion for two grid studies. The first study addresses the grid density independence. Both C-grids extend 0.92 chords upstream and 0.7 chords downstream, with 157 × 22 and 313 × 40 grid points respectively. As shown in Fig. 4, there is no difference in the results. Thus, the coarser grid (Fig. 2b) is considered adequate.

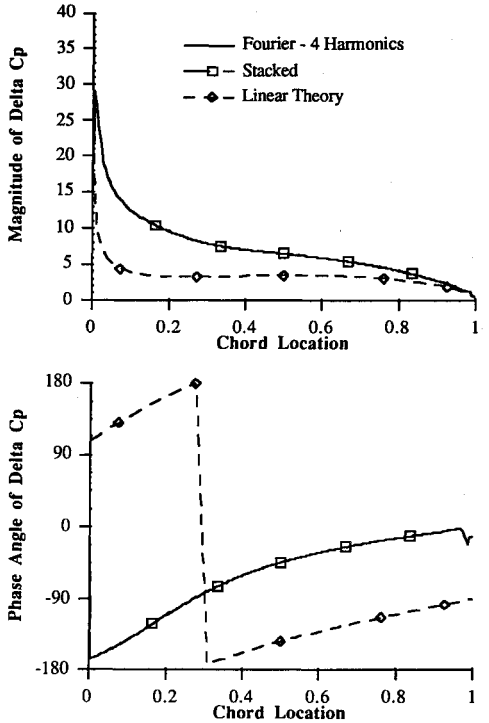

Fig. 5 10th standard configuration unsteady pressure difference. M = 0.7, k = 0.75, ζ = 45 deg, α = 10 deg, p/P_0 = 0.87, h_1 = 0.01, C/S = 1.0, σ = −45 deg.

The second study is performed to determine grid independence from effects at the inlet and exit plane. The C-grid was extended to 1.5 chords upstream of the leading-edge plane and to 2.0 chords downstream of the trailing-edge plane with 289 × 31 points in the grid. The same subsonic translational zero interblade phase angle configuration was analyzed. Note that this is a super-resonant cascade flow configuration, with planar propagating waves generated. For a super-resonant

cascade, acoustic waves do not decay as they propagate away from the oscillating cascade. Therefore, a super resonance condition should be the most sensitive to the inlet and exit location. The results are also shown in Fig. 4. No boundary reflection problem is evident, although for nonplanar waves a reflection may occur. Therefore, the smaller grid is utilized.

The subsonic 10th standard configuration cascade airfoil surface unsteady pressure difference magnitude and phase response to a translational motion of 1% chord at an interblade phase angle of −45 deg is shown in Fig. 5. Both the Fourier and stacked periodic boundary conditions results are shown, along with the linear flat plate theory analysis of Whitehead.[1] The two nonlinear analysis results are identical in both magnitude and phase. The magnitude of the Euler unsteady response is three times higher near the leading edge, with the difference decreasing until the Euler and linear solutions agree at the trailing edge. The phase results show that the Euler and linear solutions have the same trendwise behavior, but are offset by 90 deg.

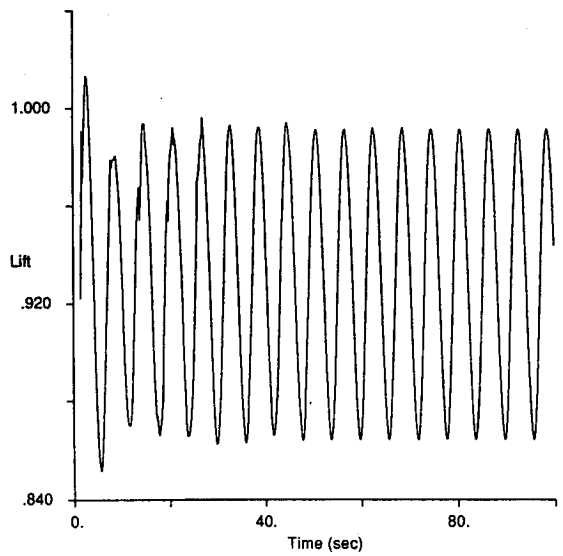

Fig. 6 Lift time history.

The time history of the unsteady lift for the Fourier periodic boundary condition Euler analysis is shown in Fig. 6. This plot shows that the solution has reached a periodic state after 12 periods of oscillation. This takes 6.4 CPU h on the HP-730, whereas the stacked analysis reached a periodic state in 4 periods taking 16.5 CPU h. The Fourier periodic boundary condition analysis probably takes longer to reach a periodic state because the boundary conditions are lagged in time, whereas the stacked boundary conditions are not.

The importance of the number of harmonics in the Fourier periodic boundary conditions is shown in Fig. 7. The magnitude of the first eight harmonics of the conservative variable ρu normalized by the first harmonic from the stacked analysis is shown for five different node locations along the periodic boundary. The Fourier periodic boundary conditions were used, with both the first and the first four harmonics used to determine the solution at the periodic boundary. The magnitude of the harmonics do not change whether the first or the first four terms are kept, i.e., the periodic boundary solution is dominated by the first harmonic.

Transonic Cascade

To demonstrate the Fourier periodic boundary conditions for transonic flow, a cascade configuration with a strong normal shock was analyzed. The 10th standard configuration geometry was used with a freestream Mach number of 0.8. The back pressure was reduced to 0.7, resulting in a strong shock wave completely across the flow passage. The number of grid points in the streamwise direction was increased to 223 to better resolve the shock wave, but no grid refining near the shock was done.

The flowfield static pressure contours are presented in Fig. 8, showing that the normal shock extends completely across the blade passage. The steady pressure distribution on the suction and pressure surfaces of the cascade are given in Fig. 9. The shock starts at 92% chord on the suction surface and intersects the pressure surface at 25% chord.

The cascade is then oscillated in a torsional mode about the midchord with a −90-deg interblade phase angle. The

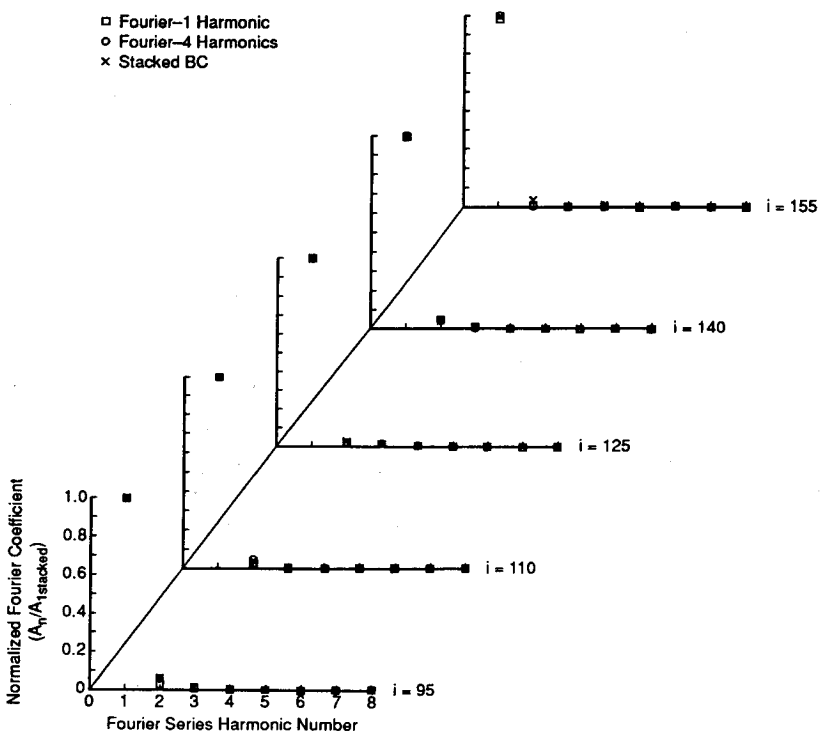

Fig. 7 Normalized ρu Fourier series harmonic amplitudes. $M = 0.7$, $k = 0.75$, $\zeta = 45$ deg, $\alpha = 10$ deg, $p/P_0 = 0.87$, $h_1 = 0.01$, $C/S = 1.0$, $\sigma = -45$ deg.

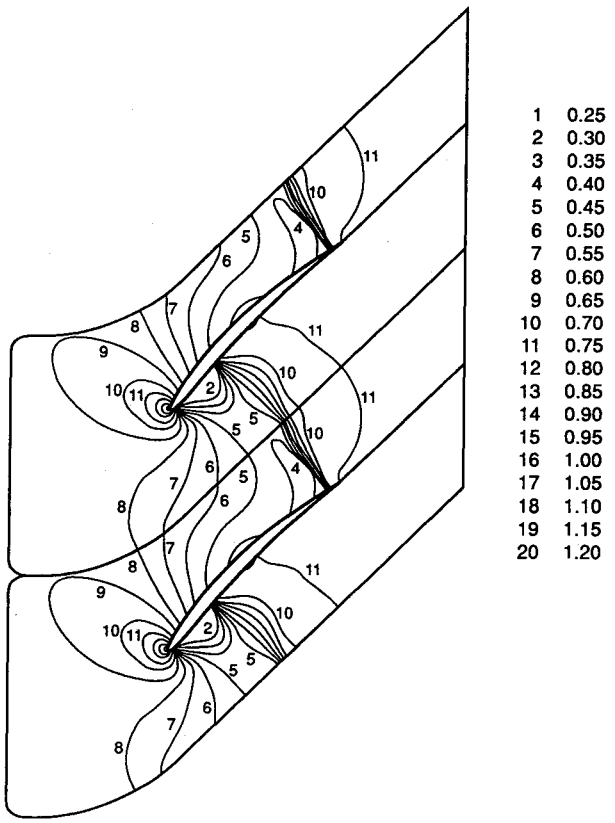

Fig. 8 10th standard configuration static pressure contours. $M = 0.8$, $\zeta = 45$ deg, $\alpha = 10$ deg, $C/S = 1.0$, $p/P_0 = 0.7$.

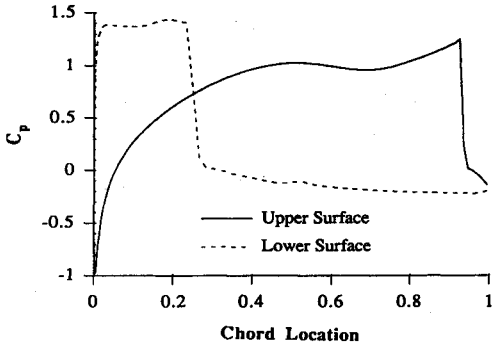

Fig. 9 10th standard configuration steady pressure distribution. $M = 0.8$, $\zeta = 45$ deg, $\alpha = 10$ deg, $C/S = 1.0$, $p/P_0 = 0.7$.

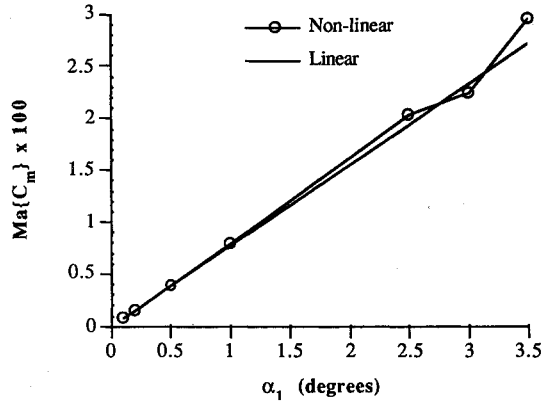

Fig. 10 Unsteady moment coefficient vs amplitude of oscillation. $M = 0.8$, $k = 0.75$, $\zeta = 45$ deg, $\alpha = 10$ deg, $p/P_0 = 0.7$, $C/S = 1.0$, $\sigma = -90$ deg.

amplitude of the airfoil oscillation is varied from 0.1 to 3.5 deg. The magnitude of the unsteady moment coefficient from the 0.1- and 0.2-deg oscillations are extrapolated for the "linear" solution. The unsteady moment coefficient is then plotted vs the amplitude of oscillation (Fig. 10). Nonlinear effects are evident for oscillation amplitudes greater than 1.0 deg. This result agrees with studies on nonlinear cascade effects reported in Ref. 18.

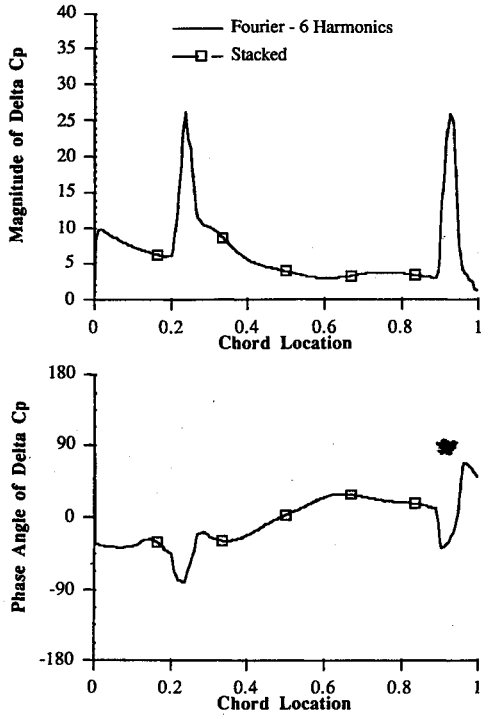

Fig. 11 10th standard configuration unsteady pressure difference. $M = 0.8$, $k = 0.75$, $\zeta = 45$ deg, $\alpha = 10$ deg, $p/P_0 = 0.7$, $\alpha_1 = 3.5$ deg, $C/S = 1.0$, $\sigma = -90$ deg.

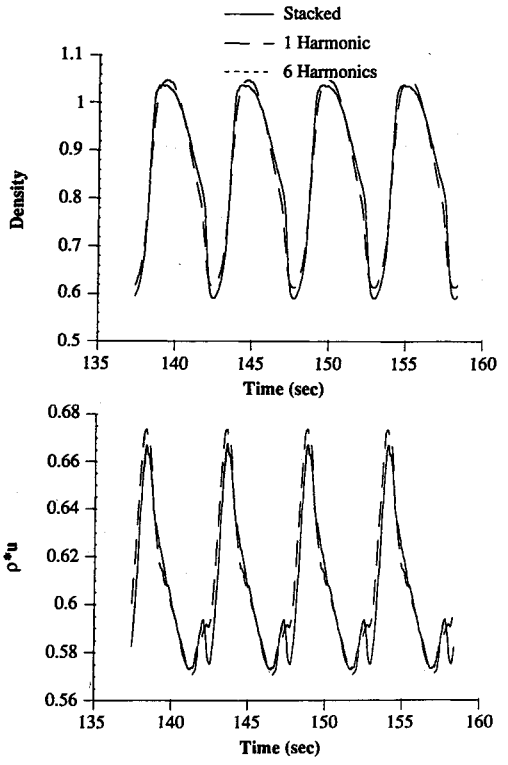

Fig. 12 Time trace of conservative variables at periodic boundary. $M = 0.8$, $k = 0.75$, $\zeta = 45$ deg, $\alpha = 10$ deg, $p/P_0 = 0.7$, $\alpha_1 = 3.5$ deg, $C/S = 1.0$, $\sigma = -90$ deg.

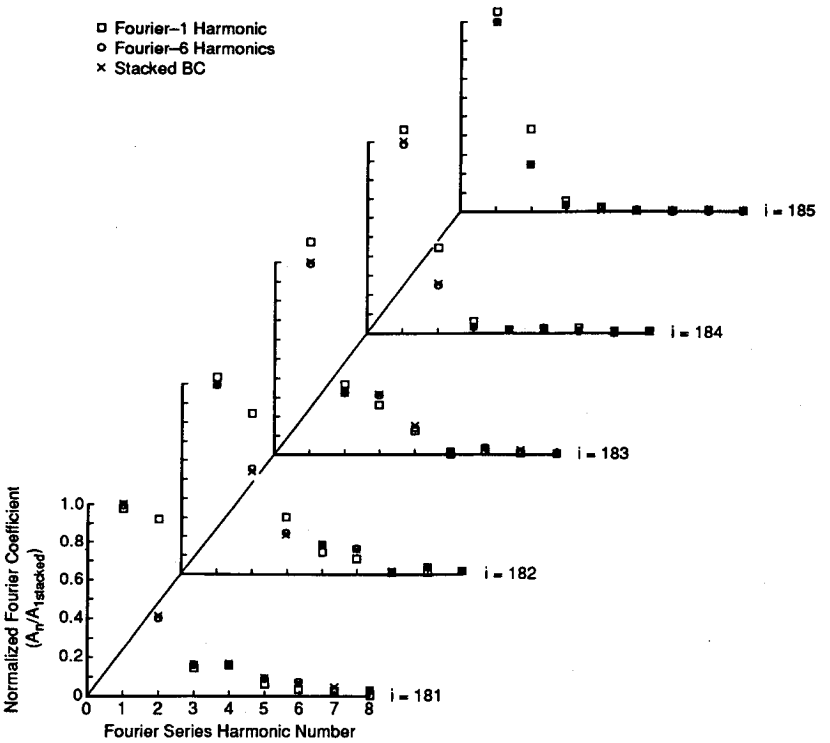

Fig. 13 Normalized ρu Fourier series harmonic amplitudes. $M = 0.8$, $k = 0.75$, $\zeta = 45$ deg, $\alpha = 10$ deg, $p/P_0 = 0.7$, $\alpha_1 = 3.5$ deg, $C/S = 1.0$, $\sigma = -90$ deg.

Figure 11 shows the airfoil surface unsteady pressure magnitude and phase results for an oscillation amplitude of 3.5 deg for both the stacked and Fourier periodic boundary conditions, with the first six harmonics used for the Fourier method. The unsteady magnitude and phase pressure response are identical for both methods. The strong normal shock is seen in both the magnitude and phase plots at 25 and 92% chord, with this nonlinear behavior able to be calculated with the Fourier periodic method. The CPU time was 147.0 and 238.8 h on the HP-730 for the Fourier and stacked periodic boundary conditions, respectively, with 35 and 15 periods of oscillation required to reach a periodic solution.

To investigate the Fourier periodic boundary condition solution in more detail, the time history of the conservative variables ρ and ρu, one node in from the periodic boundary at the shock wave location, are plotted in Fig. 12 for both the stacked periodic boundary condition and for the prediction with both the first and the first six harmonics of the Fourier periodic boundary condition method. Only the last four periods of oscillation are plotted to give better resolution. Although the first harmonic alone boundary condition does remarkably well, using the first six harmonics in the boundary condition yields a solution that is nearly identical to that with the stacked airfoils.

The magnitude of the first eight Fourier coefficients one node in from the periodic boundary for the conservative variable ρu at the normal shock location, and for the two nodes upstream and downstream of the shock location, are shown in Fig. 13. Note, these plots are for an internal node point, thus higher harmonic terms result. Nearly exact agreement between the solution with the stacked and Fourier periodic boundary condition using the first six terms result. However, it is evident that using only the first term in the boundary condition does not maintain the higher harmonic effect at the flowfield periodic boundary. This figure also emphasizes the validity of only keeping the first six harmonics of the boundary condition, as the higher harmonics are quite small. These results validate that the Fourier periodic boundary conditions preserve the nonlinear behavior of the flow solver.

CPU Time

The CPU time penalty due to the timewise integrations for the first six harmonics of the Fourier series along the periodic boundaries for a single passage was 2.7 min or 5.6% of the 48.5 min required for one period of oscillation of a transonic 10th standard configuration for a zero interblade phase angle analysis with overlapping of the grid. The number of oscillations needed to reach a periodic solution was usually double that needed for the stacked periodic boundary conditions. Therefore, depending on the interblade phase angle, the savings in CPU time can be enormous. Also, any arbitrary interblade phase angle can easily be analyzed. The penalty in terms of memory requirements for a particular cascade flowfield analysis was approximately 3.0% of the stacked boundary condition. This should not pose any problem for most modern computers.

Summary and Conclusions

An investigation of the unsteady aerodynamics associated with an oscillating cascade of airfoils has been completed using a time-marching, flux-difference splitting Euler code implemented on a deforming C-grid. The flow solver, which is second-order accurate in time and third-order accurate spatially, was first verified by analyzing a flat plate cascade and comparing the results with linear theory. This showed excellent agreement with the linear theory predictions, thus validating the flow solver. The 10th standard cascade configuration was then analyzed. As expected, these predictions showed effects that the linear theory could not predict, and they showed the usefulness of applying the Fourier periodic boundary conditions in saving computer resources. To prove the nonlinear validity of the Fourier periodic boundary conditions, a transonic cascade configuration with a strong normal shock wave and high magnitudes of torsional blade oscillation was studied. These results proved the nonlinear behavior of the Fourier periodic boundary conditions.

The conclusion of this research into the nonlinear unsteady aerodynamics of a cascade of airfoils undergoing both trans-

lational and torsional oscillation is that applying a Fourier periodic boundary condition is valid. This periodic boundary condition has been demonstrated to model the nonlinear behavior of the flowfield while greatly reducing the computer resources in both time and memory requirements over other methods.

Acknowledgments

Research sponsored by the Air Force Office of Scientific Research, Contract AFOSR-91-0251. The authors would like to acknowledge Dan Fant, program manager, for his support throughout the course of this investigation, and Dennis Huff, NASA Lewis Research Center, for providing the basic flow algorithm.

References

[1]Whitehead, D. S., "Classical Two-Dimensional Methods," *Unsteady Turbomachinery Aerodynamics*, Vol. 1, 1987, pp. 3-1–3-29.

[2]Verdon, J. M., "Linearized Unsteady Aerodynamic Theory," *Unsteady Turbomachinery Aerodynamics*, Vol. 1, 1987, pp. 2-1–2-31.

[3]Giles, M. B., and Haimes, R., "Validation of a Numerical Method for Unsteady Flow Calculations," American Society of Mechanical Engineers Paper 91-GT-271, June 1991.

[4]Gerolymos, G. A., "Numerical Integration of the 3D Unsteady Euler Equations for Flutter Analysis of Axial Flow Compressors," American Society of Mechanical Engineers Paper 88-GT-255, June 1988.

[5]Huff, D. L., "Numerical Simulations of Unsteady, Viscous, Transonic Flow over Isolated and Cascaded Airfoils Using a Deforming Grid," AIAA Paper 87-1316, June 1987.

[6]Huff, D. L., and Reddy, T. S. R., "Numerical Analysis of Supersonic Flow Through Oscillating Cascade Sections by Using a Deforming Grid," AIAA Paper 89-2805, July 1989.

[7]Erdos, J. I., Alzner, E., and McNally, W., "Numerical Solution of Periodic Transonic Flow Through a Fan Stage," *AIAA Journal*, Vol. 15, No. 11, 1977, pp. 1559–1568.

[8]Giles, M. B., "Calculation of Unsteady Wake Rotor Interaction," *Journal of Propulsion and Power*, Vol. 4, No. 4, 1988, pp. 356–362.

[9]He, L., "An Euler Solution for Unsteady Flows Around Oscillating Blades," American Society of Mechanical Engineers Paper 89-GT-279, June 1989.

[10]Whitfield, D. L., Janus, J. M., and Simpson, L. B., "Implicit Finite Volume High Resolution Wave-Split Scheme for Solving the Unsteady Three-Dimensional Euler and Navier-Stokes Equations on Stationary or Dynamic Grids," Mississippi State Engineering and Industrial Research Station, Rept. MSSU-EIRS-ASE-88-2, Mississippi State, MS, Feb. 1988.

[11]Janus, J. M., "Advanced 3-D CFD Algorithm for Turbomachinery," Ph.D. Dissertation, Mississippi State Univ., Mississippi State, MS, May 1989.

[12]Huff, D. L., "Numerical Analysis of Flow Through Oscillating Cascade Sections," AIAA Paper 89-0437, Jan. 1989.

[13]Sorenson, R. L., "A Computer Program to Generate Two-Dimensional Grids About Airfoils and Other Shapes by the Use of Poisson's Equation," NASA TM 81198, April 1981.

[14]Chima, R. V., "Explicit Multi-Grid Algorithm for Quasi Three-Dimensional Viscous Flow in Turbomachinery," *Journal of Propulsion and Power*, Vol. 3, No. 5, 1987, pp. 397–405.

[15]Janus, J. M., "The Development of a Three-Dimensional Split Flux Vector Solver with Dynamic Grid Applications," M.S. Thesis, Mississippi State Univ., Mississippi State, MS, Aug. 1984.

[16]Giles, M. B., "Non-Reflecting Boundary Conditions for Euler Equation Calculations," *AIAA Journal*, Vol. 28, No. 12, 1990, pp. 2050–2058.

[17]Fransson, T. H., and Verdon, J. M., "Panel Discussion on Standard Configurations for Unsteady Flow Through Vibrating Axial-Flow Turbomachine-Cascades," *Sixth International Symposium on Unsteady Aerodynamic, Aeroacoustics and Aeroelasticity of Turbomachines and Propellers*, Springer-Verlag, Univ. of Notre Dame, Notre Dame, IN, 1991, pp. 859–889.

[18]Huff, D. L., Swafford, T. W., and Reddy, T. S. R., "Euler Flow Predictions for an Oscillating Cascade Using a High Resolution Wave-Split Scheme," NASA TM 104377, June 1991.